Developing Green, Highly Flowable, Rapid Set, High-Performance Concrete for Pavement Patch Repair

Final Report
July 2016

Sponsored by
Iowa State University
Midwest Transportation Center
U.S. Department of Transportation
Office of the Assistant Secretary for
Research and Technology

IOWA STATE UNIVERSITY
Institute for Transportation

About MTC

The Midwest Transportation Center (MTC) is a regional University Transportation Center (UTC) sponsored by the U.S. Department of Transportation Office of the Assistant Secretary for Research and Technology (USDOT/OST-R). The mission of the UTC program is to advance U.S. technology and expertise in the many disciplines comprising transportation through the mechanisms of education, research, and technology transfer at university-based centers of excellence. Iowa State University, through its Institute for Transportation (InTrans), is the MTC lead institution.

About InTrans

The mission of the Institute for Transportation (InTrans) at Iowa State University is to develop and implement innovative methods, materials, and technologies for improving transportation efficiency, safety, reliability, and sustainability while improving the learning environment of students, faculty, and staff in transportation-related fields.

ISU Non-Discrimination Statement

Iowa State University does not discriminate on the basis of race, color, age, ethnicity, religion, national origin, pregnancy, sexual orientation, gender identity, genetic information, sex, marital status, disability, or status as a U.S. veteran. Inquiries regarding non-discrimination policies may be directed to Office of Equal Opportunity, Title IX/ADA Coordinator, and Affirmative Action Officer, 3350 Beardshear Hall, Ames, Iowa 50011, 515-294-7612, email eooffice@iastate.edu.

Notice

The contents of this report reflect the views of the authors, who are responsible for the facts and the accuracy of the information presented herein. The opinions, findings and conclusions expressed in this publication are those of the authors and not necessarily those of the sponsors.

This document is disseminated under the sponsorship of the U.S. DOT UTC program in the interest of information exchange. The U.S. Government assumes no liability for the use of the information contained in this document. This report does not constitute a standard, specification, or regulation.

The U.S. Government does not endorse products or manufacturers. If trademarks or manufacturers' names appear in this report, it is only because they are considered essential to the objective of the document.

Quality Assurance Statement

The Federal Highway Administration (FHWA) provides high-quality information to serve Government, industry, and the public in a manner that promotes public understanding. Standards and policies are used to ensure and maximize the quality, objectivity, utility, and integrity of its information. The FHWA periodically reviews quality issues and adjusts its programs and processes to ensure continuous quality improvement.

Technical Report Documentation Page

1. Report No.	2. Government Accession No.	3. Recipient's Catalog No.

4. Title and Subtitle	5. Report Date
Developing Green, Highly Flowable, Rapid Set, High-Performance Concrete for Pavement Patch Repair	July 2016
	6. Performing Organization Code

7. Author(s)	8. Performing Organization Report No.
Kejin Wang and Gilson R. Lomboy	

9. Performing Organization Name and Address	10. Work Unit No. (TRAIS)
Institute for Transportation Iowa State University 2711 South Loop Drive, Suite 4700 Ames, IA 50010-8664	**11. Contract or Grant No.** DTRT13-G-UTC37

12. Sponsoring Organization Name and Address		13. Type of Report and Period Covered
Midwest Transportation Center 2711 S. Loop Drive, Suite 4700 Ames, IA 50010-8664 Civil, Construction, & Environmental Engineering, Iowa State University 394 Town Engineering, Ames, IA 50011	U.S. Department of Transportation Office of the Assistant Secretary for Research and Technology 1200 New Jersey Avenue, SE Washington, DC 20590	Final Report **14. Sponsoring Agency Code**

15. Supplementary Notes

Visit www.intrans.iastate.edu for color pdfs of this and other research reports.

16. Abstract

A high-performance mortar (HPM) containing a large amount of industrial by-products such as fly ash, silica fume, and limestone fines was developed for rapid repair of concrete pavements. The HPM development included three major steps.

1. Development of the mortar mixture proportion based on the optimal hydration of binder and particle packing of the mortar system. In this step of the study, all mortar materials were systematically proportioned, and the obtained mixtures were tested for flowability, rate of hydration, set time, and strength development. The optimal mixture proportion was then selected as the HPM, as it displayed good self-consolidating ability and achieved 1-day compressive strengths greater than 6,000 psi.

2. Investigation of the mechanical properties of the new HPM, including compressive and flexural strength, elastic modulus, and slant shear and pull-off strengths of patch-substrate bonds tested at 1, 3, 7, and 28 days. In this step, the properties of the HPM were evaluated in comparison with those of a commercial repair material: the rapid-set concrete (RSC). Two types of substrates representing old concrete were used for patching repair. One was made of a typical pavement mixture (C-3WR-C20), and the other was a high-strength pavement concrete mixture (O-4WR).

3. Investigation of the durability properties of the newly developed HPM compared to those of the RSC. Durability properties included cyclic freeze-thaw (F-T) resistance, permeability, and shrinkage behavior.

The results indicated that the newly developed HPM possesses excellent self-consolidating ability: highly flowable and non-segregating. Although there was delayed setting, the compressive strength of the HPM exceeded 6,000 psi at 1 day, approximately 25 percent higher than that of the RSC. At 28 days, the HPM reached 10,000 psi, while the RSC was about 7,000 psi. The HPM also displayed extremely low chloride permeability (18 coulombs) compared to the RSC (2,550 coulombs) and excellent F-T durability without the requirement for air entrainment. The F-T durability factor of HPM was kept around 100% throughout the standard F-T test, while the F-T durability factor of RSC reduced to 80% at the end of the F-T test. However, the HPM exhibited noticeably higher autogenous shrinkage and slightly lower free drying shrinkage than the C-3WR-C20 mixture, while the RSC had a little/no shrinkage during the 56-day test period. Addition of a small amount of micro-steel fibers (70 pcy) slightly reduced the shrinkage of the HPM.

Further studies on fatigue and shrinkage cracking behavior of the HPM are recommended.

17. Key Words	18. Distribution Statement
concrete pavement patches—high-performance mortar—limestone fines—rapid repair	No restrictions.

19. Security Classification (of this report)	20. Security Classification (of this page)	21. No. of Pages	22. Price
Unclassified.	Unclassified.	52	NA

Form DOT F 1700.7 (8-72) **Reproduction of completed page authorized**

DEVELOPING GREEN, HIGHLY FLOWABLE, RAPID SET, HIGH-PERFORMANCE CONCRETE FOR PAVEMENT PATCH REPAIR

Final Report
July 2016

Principal Investigator
Kejin Wang, Professor
Civil, Construction, and Environmental Engineering, Iowa State University

Co-Principal Investigator
Gilson R. Lomboy, Postdoctoral Research Associate
Civil, Construction, and Environmental Engineering, Iowa State University

Research Assistants
Jiaxi Ren, Jennifer Davis, Lian Bo, and Wenjing Cai

Authors
Kejin Wang and Gilson R. Lomboy

Sponsored by
Midwest Transportation Center,
U.S. Department of Transportation
Office of the Assistant Secretary for Research and Technology,
and Civil, Construction, and Environmental Engineering
at Iowa State University

A report from
Institute for Transportation
Iowa State University
2711 South Loop Drive, Suite 4700
Ames, IA 50010-8664
Phone: 515-294-8103 / Fax: 515-294-0467
www.intrans.iastate.edu

TABLE OF CONTENTS

LIST OF FIGURES

LIST OF TABLES

ACKNOWLEDGMENTS

The authors would like to thank the Midwest Transportation Center, the U.S. Department of Transportation Office of the Assistant Secretary for Research and Technology, and the Civil, Construction, and Environmental Engineering Department at Iowa State University for sponsoring this research. The authors would also like to acknowledge the special technical and administrative support of the National Concrete Pavement Technology (CP Tech) Center at Iowa State University's Institute for Transportation throughout the entire project.

Visiting Professor An Cheng from the Department of Civil Engineering at the National Ilan University in Taiwan was involved in the early-stage testing of various potential rapid repair concrete mixtures during his three-month stay at Iowa State University. Visiting Professor Zhiqing Zhang assisted in the freeze-thaw (F-T) cycle testing and preparation of the mixtures for the research. Brian Batten of BASF Master Builders Solutions contributed materials for the project: high-range and normal-range water reducers and silica fume. The project would not have been successfully completed without the support of the above-mentioned researchers and the hard work of research assistants Jiaxi Ren, Jennifer Davis, Lian Bo, and Wenjing Cai.

1 INTRODUCTION

1.1 Background

The United States has an aging transportation infrastructure that is requiring extensive maintenance. According to a survey by The Road Information Program, 32 percent of major roads in the US are in either poor or mediocre condition (TRIP 2012). Rapid repair of the deteriorated roads is essential to avoiding the inconvenience of commuters and disruption of daily business. The repaired pavements must be strong and durable to meet service requirements and extend their service lives. For these demands, use of high-performance concrete (HPC) as a repair material is a very attractive option.

HPC has been increasingly used for transportation structures, and especially bridge decks. HPC features the following qualities: high early strength (approximately 4,000 psi at 24 hours), high workability, and high durability.

Recently, research has revealed that ultra-high-strength concrete (UHSC) or ultra-high-performance concrete (UHPC) can be produced using quartz and quartzite powders. Such concrete has very good flowability and excellent strengths (22,000 psi at 28 days). Unfortunately, the existing UHPC is often specially formulated and packaged with particular materials, and it is expensive and difficult to be directly produced by users. In addition, most existing UHPC is not designed to have features for concrete repair, which includes not only rapid set and early compressive strength but also excellent workability, bond strength, shrinkage, and freeze-thaw (F-T) resistance.

Research has shown that limestone powders can benefit concrete in many ways: (1) chemically, by supplying ions that modify the kinetics of hydration and the morphology of hydration products (Daimon and Sakai 1998) while very fine limestone particles can act as nucleation sites, thereby accelerating strength development (Sato and Diallo 2010); (2) physically, by assisting cement grain dispersion and enhancing packing density, thus reducing the interstitial voids and permeability (Hornain 1995) and increasing concrete fluidity (Moir and Kelham 1997); (3) economically, because limestone fine-based HPC can reduce the life-cycle cost by using less cement and increasing strength and durability (Baron and Douvre 1987); and (4) ecologically, because using less cement can decrease carbon dioxide and mono-nitrogen oxide emissions and save fossil fuels and mineral resources (Bonavetti et al. 2003).

Based on the particle packing principle, each large particle in a cement-based system shall be surrounded by one or more layers of smaller-sized particles: the inert granular particles are surrounded by cementitious materials and the unhydrated cementitious grains are then coated with cementitious hydration products (see Figure 1).

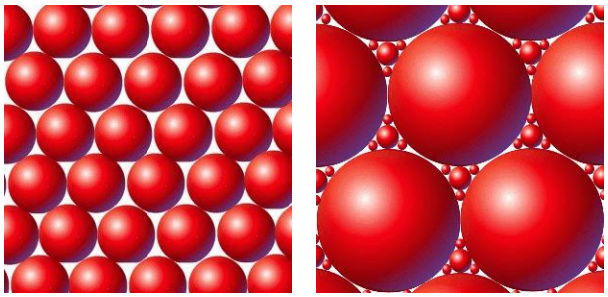

TecEco Pty. Ltd.

Figure 1. Single size particle packing (left) and three size particle packaging (right)

Such particle packing helps the uniform distribution of cementitious materials, thereby accelerating their hydration. As shown in Figure 2, instead of the skeleton where the forces are transmitted at the aggregate interfaces in normal strength concrete (NSC), small aggregate particles for ultra-high-performance concrete become inclusions in a continuous matrix.

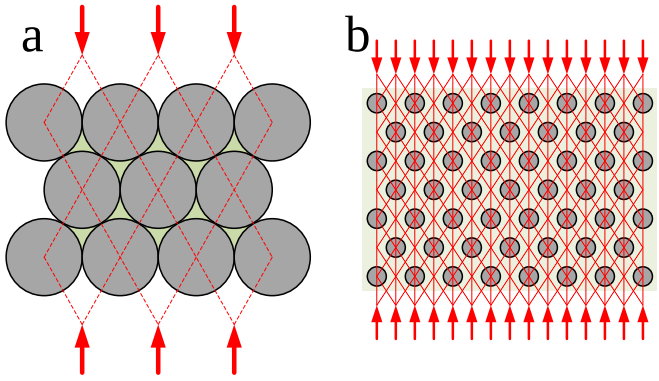

Walraven 2002

Figure 2. Force transfer in normal strength concrete (left) and in ultra-high-performance concrete (right)

The stress at the aggregate interface is greatly reduced and the forces are transmitted more uniformly (Richard and Cheyrezy 1995, Schmidt et al. 2003, Schmidt and Fehling 2005) to produce stronger concrete.

In this research, we developed high-performance mixtures utilizing limestone fines (LF), a by-product from the aggregate industry, as a pavement repair material. Our approach to the development of a new high-performance mixture was based on the chemical interactions and particle packing of concrete materials. The materials studied mainly included portland cement (PC), fly ash (FA), limestone fines (LF), silica fume (SF), and river sand (RS). In addition, a high-range water reducer (HRWR) was used to improve the self-consolidating ability of the concrete. Our rationale was that these individual materials have different chemistry and particle size distributions and could integrate and compensate each other to form a new material with optimal chemistry and density. Through synergizing these materials and tailoring their mix

proportions, the new high-performance mixture has the ability to self-consolidate, has high early strength, excellent bond strength with substrates, and long-term durability.

1.2 Objectives

Our approach to the above-mentioned limestone fines-based, rapid set, high-performance mortar (HPM) development is based on the chemical interactions and particle packing of materials. In this study, the focus was mixture design development and laboratory performance evaluation. The following specific objectives were pursued in the study:

1. To study the chemical and physical interactions between limestone fines, cementitious materials, and chemical admixtures
2. To develop a mix design methodology for a HPM, based on the optimization of the chemical and physical particle interactions
3. To evaluate the key mechanical and durability properties of the HPM
4. To investigate the applicability and performance of the HPM for concrete repair

1.3 Scope

The study was divided into three steps. The first step was the development of mix proportion. During this step, mortar materials were collected and characterized. Systematic combinations of the materials were tested to obtain mixtures with good flowability, rate of hydration, setting time, and strength development. The materials characterization is presented in Section 2. The mixture proportioning is discussed in Section 3. The second step was to investigate the mechanical properties of the newly developed rapid repair patch material. The compressive and flexural strength, elastic modulus, and patch-substrate bonds were tested. These are discussed in Section 4. In the third step, the durability properties of the newly developed rapid repair material were investigated. The cyclic freeze-thaw resistance, permeability, and shrinkage behavior were measured and are presented in Section 5. Finally, the conclusions and recommendations of this research can be found in Section 6.

2 MATERIALS AND MIXING METHODS

2.1 Materials

The materials considered for the development of the HPM are Type I portland cement, silica fume, Class F fly ash, limestone fines, and river sand. The particle size distributions of the fine materials measured by laser diffraction are shown in Figure 3.

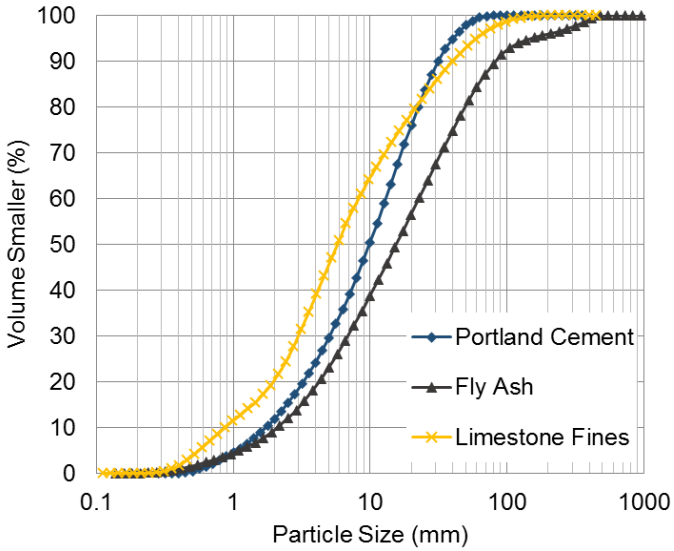

Figure 3. Particle size distribution of portland cement, fly ash, and limestone fines

In the case of silica fume particles, their very small size makes them susceptible to agglomeration. This makes the measured size distribution dependent on the degree of dispersion achieved. The size distributions of the SF used in this study, at three different degrees of dispersion, are presented in Figure 4.

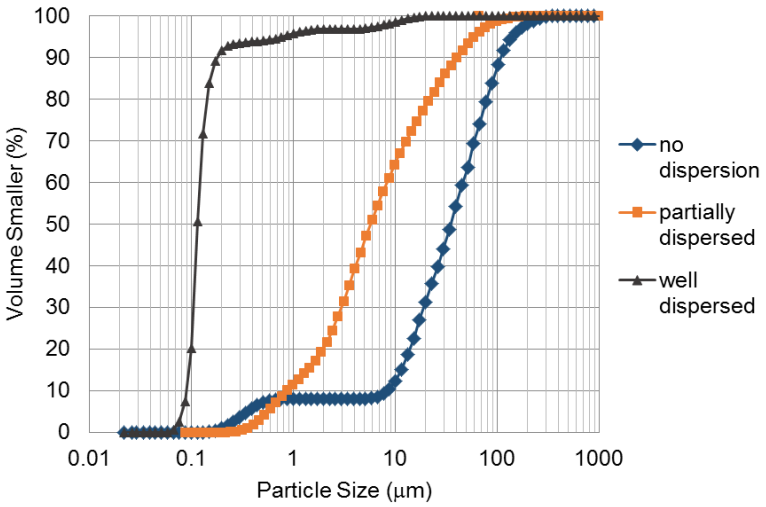

Figure 4. Particle size distribution of SF tested by laser diffraction under three degrees of dispersion: no dispersion – tested as is, partially dispersed – sonicated with surfactant, and well dispersed – sonicated for 180 seconds with surfactant

The first test involved measuring without applying any dispersion method on the SF sample (no dispersion). The second test was sonicated with a surfactant (partially dispersed). The third was sonicated for 180 seconds (well dispersed). The average particle size of the SF is often reported as 0.1 μm. The average particle sizes measured with no dispersion, partially dispersed, and well-dispersed conditions are 34.25 μm, 5.92 μm, and 0.115 μm, respectively.

The river sand particle size distribution determined by sieve analysis is given in Figure 5. The calculated fineness modulus of the RS is 3.08.

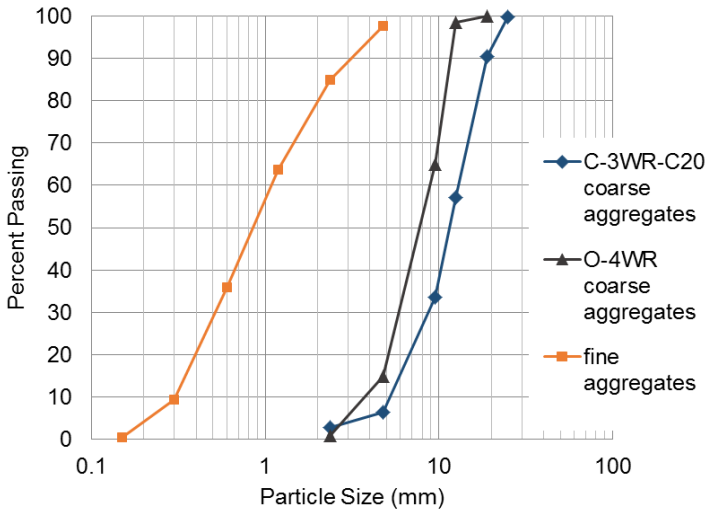

Figure 5. Gradation of coarse aggregates for substrates C-3WR-C20, O-4WR, and fine aggregates

Two types of substrates representing old concrete to be patched were used in this study. One substrate was C-3WR-C20, which is a typical pavement mixture (w/b=0.42). Another type of substrate used was O-4WR, which is a high-strength concrete mixture (w/b=0.33) used for bridge decks. The coarse aggregate for the substrates was crushed limestone. C-3WR-C20 has a 1 in. nominal maximum size aggregate (NMSA) meeting size number 57, as described in ASTM C33, while O-4WR aggregates have a 1/2 in. NMSA that meet Gradation No. 6 in the Iowa Department of Transportation Specifications. The particle size distributions of the coarse aggregates are given in Figure 5. The mix proportions of the substrates are given in Table 1. Except for Class C fly ash in the C-3WR-C20, the types of cementitious materials and fine aggregate used in the substrates are the same as those in the developed rapid repair mixture.

Table 1. Mix proportions of substrates (mature concrete to be patched)

	Cement (pcy)	Fly Ash (pcy)	Water (pcy)	River Sand (pcy)	Coarse Aggregates (pcy)	AEA (fl oz/cwt)	NRWR (fl oz/cwt)
C-3WR-C20	455.0	113.8	244.9	1363.1	1707.3	0.50	3.0
O-4WR	824.6		269.3	1381.3	1418.0	0.75	3.5

High-range water reducers, normal-range water reducers (NRWRs), and air entraining admixture (AEA) were used in the different mixtures in this research. The HRWR and NRWR used was the Glenium 7500 and Pozzolith 322N by BASF Master Builders Solutions, respectively. The air entraining admixture was AEA 92 by Euclid Chemicals. The high-range water reducer was used in the development of the rapid repair concrete. The normal range water reducer and air entraining admixture were part of the substrate mixtures.

Rapid-set concrete (RSC) mix from the CTS Cement Manufacturing Corporation was used to compare the new mixture to a commercial rapid repair material. RSC is a product that meets the Iowa Department of Transportation Materials I.M. 491.20 requirements for rapid set patch material for concrete repair. It is composed of 20 to 35 percent calcium sulfoaluminate cement and 65 to 80 percent silica sand. The recommended water for 60 pounds of RCS is 3.3 to 4.2 liters and 3.75 liters was used.

To complement the high compressive strength and improve volume stability of the newly developed rapid repair material, the addition of micro-steel fiber was explored. The micro-steel fibers were cold drawn with electroplated high-carbon steel wires and cut to form copper-coated steel straight fibers (13 mm in length and 0.2 mm in diameter) with a tensile strength of $\geq$ 2.85 GPa. Typical dosages range from 50 to 185 pounds of fiber per cubic yard of concrete.

2.2 Mixing Methods

There were three mixing methods employed in this research, which depended on the type of mixture being made. The first method is for substrate concrete C-3WR-C20 and O-4WR, which were mixed following ASTM C192. The second method is for the newly developed rapid repair

material, or high-performance mortar, which was mainly composed of fine powders and had a low water-to-binder ratio (w/b) ratio. A three-stage mixing method was developed for this new rapid repair material mixture to ensure homogeneity. The third mixing method is for the RSC. RSC begins to lose its plasticity after a few minutes of being in contact with water and therefore has to be mixed quickly. These different mixing methods are presented below.

The mixer used for preparing C-3WR-C20 and O-4WR was a 3-cf drum mixer. The mixing procedure is as follows:

1. Combine the admixtures with 3/4 of the mixing water in a container
2. Place the coarse aggregates and the 3/4 of the mixing water with admixture in the mixer
3. Start the mixer rotation to create foam for air entrainment and rotate for about 30 seconds
4. Turn off the mixer and place the fine aggregates in the mixer
5. With the mixer rotating, scoop the cementitious materials into the mixer
6. Add the remainder of the mixing water
7. After having all the ingredients in the mixer, keep the mixer rotating for 3 minutes
8. Turn off the mixer for 3 minutes and cover the open end of the mixer with a damp cloth
9. Turn on the mixer again for a final mixing of 2 minutes

The mixer for the new rapid repair material can be either a mortar power mixer or a 5-gallon pan mixer. When a mortar power mixer was used, the motor was set at 180 revolutions per minute (rpm). The mixing procedure is as follows:

1. Combine the admixtures with 3/4 of the mixing water in the mixer
2. Place the cementitious materials in the mixer with the water and admixture
3. Start the mixer and let it run for 1 minute (Stage 1)
4. Stop the mixer and add the limestone fines
5. Start the mixer and let it run for 1 minute (Stage 2)
6. Stop the mixer and add the fine aggregates
7. Start the mixer and slowly add the remaining water and, if present, slowly add steel fibers into the mixture (Stage 3)
8. When all the ingredients of the mixture are in the mixer, run mixer for 3 minutes
9. Stop the mixer for 3 minutes and cover the open end of the mixer with a damp cloth
10. Turn on the mixer again for a final mixing of 2 minutes

The mixer for the RSC was a mortar power mixer set at 180 rpm. Being a pre-mixed and bagged product, the mixing of the RSC is simple and fast. In a 5-gallon bucket, add all the pre-measured mixing water. Submerge the mixer paddle in the water and turn the mixer on. Quickly scoop or slowly pour the RSC from the opened bag. When all ingredients are in the 5-gallon bucket, continue to mix until the RSC mixture appears uniform.

3 SELECTION OF MIXTURE

3.1 Flowability and Compressive Strength

The proportion of the materials in the mixture was optimized based on flowability and 1-day compressive strength. The combinations of materials tested for optimization are given in Table 2.

Table 2. Mix proportions, flow, and 1-day compressive strength

No.	Cement	Silica Fume	Fly Ash	River Sand	Limestone Fines	HRWR (ml/g)*	Flow (in.)	$f_{c\text{-}1d}$ (psi)
1	0.88	0.12	0.00	0.654	0.654	0.056	8.82	3173
2	0.84	0.16	0.00	0.654	0.654	0.066	7.95	3528
3	0.81	0.19	0.00	0.654	0.654	0.070	7.13	3130
4	0.77	0.23	0.00	0.654	0.654	0.069	6.89	2381
5	0.81	0.15	0.04	0.654	0.654	0.056	7.83	4000
6	0.77	0.15	0.08	0.654	0.654	0.056	8.31	4268
7	0.73	0.15	0.12	0.654	0.654	0.056	7.87	2998

*g is gram of total cementitious

The amounts of the materials are given in proportion to the total amount of binders (PC, SF, and FA) in the mixture. The water-to-binder ratio of the mixtures was 0.25, and both the RS-to-binder ratio and limestone fines-to-binder ratio were 0.654. The first group, Mixes 1 through 4, had an increasing SF replacement for PC. The second group, Mixes 5 through 7, had a constant SF replacement but increasing FA replacement for PC. The optimal amount of SF was then determined based on the results of flowability and compressive strength results, as discussed below.

To evaluate these mixtures, the materials were first mixed following ASTM C305. After mixing, the flowability of the mixture was measured using a flow mold described in ASTM C230 and a smooth flat plate. The plate and mold was first moistened, and then the mold was placed at the center of the plate. The mold was then filled with the freshly mixed mortar without tamping, as shown in Figure 6.

Figure 6. Filling of mold with rapid repair mixture

The mortar was so sufficiently flowable and self-leveling that consolidation by tamping was not required. After cleaning the sides of the mold and plate of any mortar spill or drippings, the mold was lifted in a continuous vertical motion (see Figure 7). When the spread of the flowing mortar on the plate stopped, the diameter of the mortar was measured by taking the average of two perpendicular directions.

Figure 7. Flow of rapid repair mixture

The flow diameter and 1-day compressive strength results of the mixtures are given in Table 2.

In Mixes 1 through 4, the group with only SF replacement, the lowest compressive strength was obtained from Mix 4 and the highest from Mix 2. Figure 8 shows the plot of the 1-day mortar strength verses the amount of replacement of SF for PC. It can be determined from the figure that the optimum amount of SF is 15 percent.

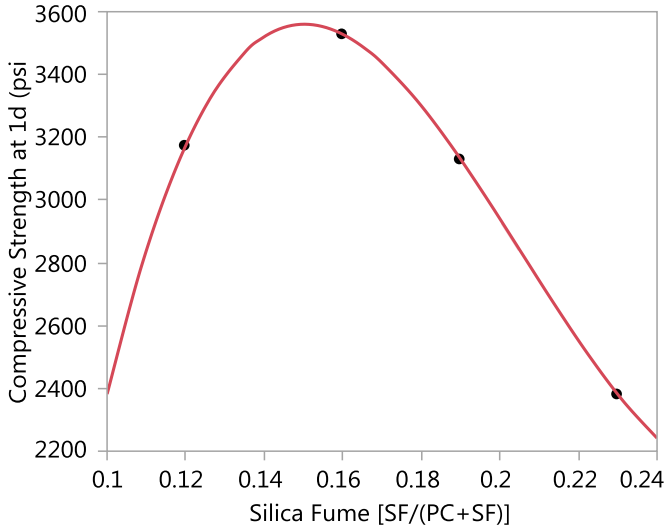

(compressive strength at 1d (psi) = 5780.3363 - 13754.167×silica fume - 197142.86×(silica fume-0.175)^2 + 2166666.7×(silica fume-0.175)^3)

Figure 8. Compressive strength of mixtures with different amounts of SF replacement

As shown in Table 2, the dosage of HRWR used in Mixes 1 through 4 increased with the increasing SF replacement. However, the flow of the mixtures still decreased with increasing replacement of SF. It is possible that the reduced strength of Mixes 3 and 4, in comparison to that of Mix 2, may be related to their reduced flowability for self-consolidation. This confirmed that the mix with 15 percent SF is considered optimal for both 1-day strength and flowability.

As SF replacement was kept as 15 percent, the effects of the amount of FA on 1-day strength and flowability on the mortar mixture were further investigated. Results from Mixes 5 through 8 in Table 2 show that further replacement of PC with FA can further increase the strength. The optimum amount of FA was found to be 8 percent, in combination with 15 percent SF replacement. The flow results were also found to be highest with the same combinations of cementitious materials. Based on the results of the compressive strength and flow tests, Mix 6 was selected for further testing as a candidate of the rapid repair material. Mix 6 is also re-designated as HPM in the rest of the report.

3.2 Particle Packing Analysis

Optimal packing of particles in cement-based mixtures generally provide the cement system with minimal porosity. In the case of concrete, an optimum packing of aggregate particles can minimize the amount of paste or binder needed to fill the space between aggregate particles. For a binder system, optimum packing of the powder materials would help improve the binder flowability by reducing the water required for filling the space between binder particles and enhance the strength of the hardened material by providing a denser microstructure and increased number of contacts between particles for continuity of load transfer.

It should be noted that sufficient lubrication should also be present between the particles to reduce interparticle friction and collision and obtain good flowability. For concrete, this lubrication between aggregate particles can result from the properties and amount of paste (binder and water). For the paste, it would be the amount of water. Since binder particles are very small and easy to agglomerate, dispersants such as a HRWR can help release the water that is trapped in the agglomerates and contribute to lubrication.

The particle packing model used in our analysis of the rapid repair mixture was the modified Andreasen & Anderson (A&A) model (Funk and Dinger 1994). The continuous packing model, expressed as the percent of volume of particles (P_t) smaller than particle size d while $d_{\max}$ and $d_{\min}$ denote maximum and minimum particle sizes, is shown in the following equation:

$$P_t = \frac{d^q - d_{\min}^q}{d_{\max}^q - d_{\min}^q} \tag{1}$$

Exponent q (the distribution modulus) controls the character of the generated mix regarding its fineness of grain. The value for q typically ranges from 0.4 to 0.5. Increasing the value of q generates an ideal packing distribution for particles with a greater number of larger-sized particles, and the opposite is true for a smaller q. When analyzing the packing of particles, the difference between the $P_{t\text{-}actual}$ (actual particle size distribution curve) and the A&A model curve (expressed as P_t) should be minimal to have optimum packing. The difference can be quantified by taking the sum of the squares of the residuals between the two curves. This can be expressed as the following equation:

$$RSS = \sum \left(P_{t-actual} - P_t \right)^2 \tag{2}$$

In the packing analysis of Mixes 1 through 7 in Table 2, the maximum particle size is taken as the nominal maximum size of the combined materials/particles. The nominal maximum size is typically the particle size within range of 95 to 85 percent of P_t. The actual nominal maximum size of the actual material is thus taken as the size at 90 percent of $P_{t\text{-}actual}$.

The particle size distribution curves of the combined powders containing PC, SF, and LF in Mixes 1 through 4 are given in Figure 9.

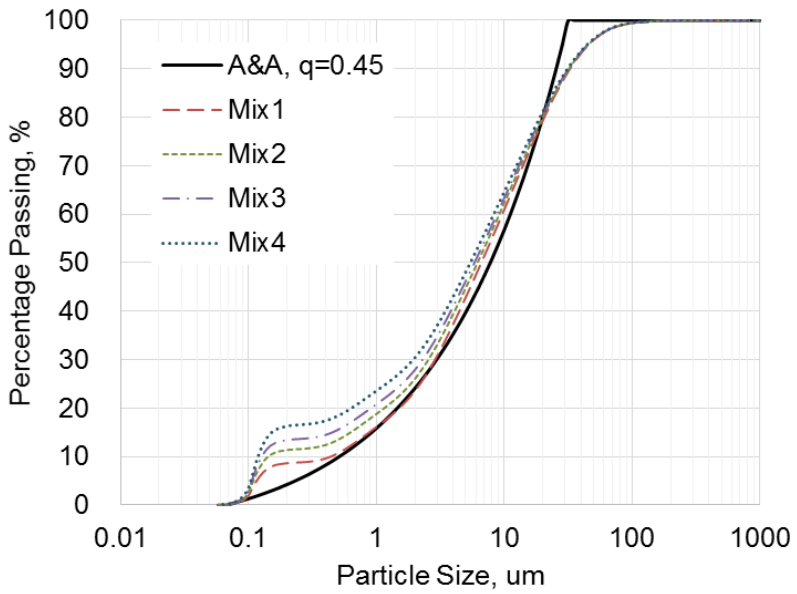

Figure 9. Particle size distribution of combined powders containing PC, SF, and LF for Mixes 1 through 4 and the A&A model

Using the A&A model curve where q=0.45 as a reference distribution, it can be observed that the increase in SF replacement causes an upward shift in the $P_{t\text{-}actual}$ curve due to an increase in finer particles. It can be reasoned that as $P_{t\text{-}actual}$ shifts upward, it may fit a better distribution when P_t has a lower q (e.g., q<0.45). Thus, Table 3 lists the distribution modulus for P_t that gives a minimum residual sum of squares (*RSS*) for the $P_{t\text{-}actual}$ of a mix and the corresponding *RSS*.

Table 3. Distribution modulus for P_t that gives a minimum *RSS* for the $P_{t\text{-}actual}$ of a mix and the corresponding *RSS*

Mix No.	*q*	RSS
1	0.42	592
2	0.38	710
3	0.34	862
4	0.30	1139
5	0.39	667
6	0.39	659
7	0.39	654

It can then be concluded that, with increasing SF replacement for PC, the distribution modulus that best describes the particle packing with the A&A model should be lower, and the increasing value of *RSS* in Mixes 1-4 indicates a decreasing packing of particles with SF replacement. It can also be suggested that the reduction in packing may also contribute to the reduction in flow and in early age strength that was obtained in the flowability and 1-day compressive strength tests.

This infers that the high compressive strength at 16 percent SF replacement is mainly due to SF's high pozzolanic reactivity, rather than contributions from the particle packing.

The particle size distribution curves of Mix 2 and Mixes 5 through 7 with the A&A model curve (q=0.39) are shown in Figure 10.

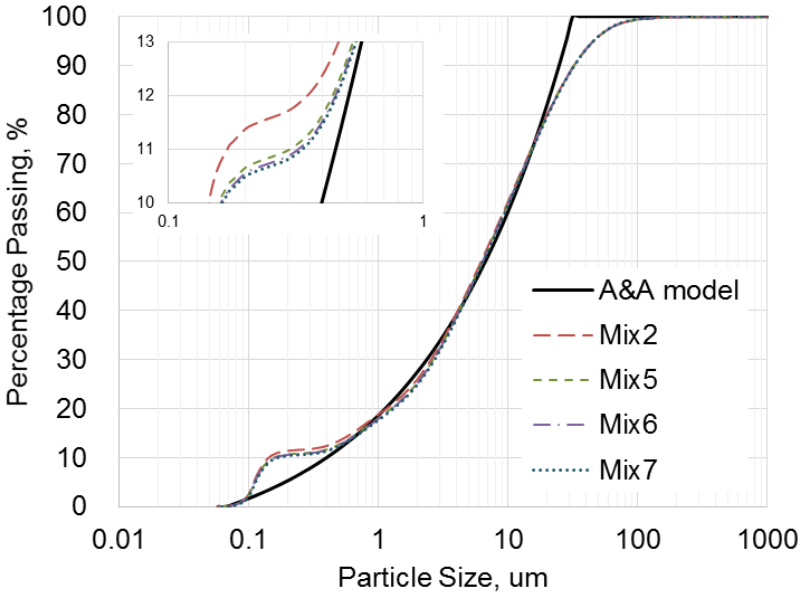

Figure 10. Particle size distribution of combined powders containing PC, SF, FA, and LF for Mix 2, Mixes 5 through 7, and the A&A model with magnified region inset

The distribution modulus that leads to a minimum *RSS* for Mixes 5 through 7 is equal to 0.39. The *RSS* values for Mixes 5 through 7 are also in Table 3. It can be seen that the inclusion of FA in the mortar mixtures (Mixes 5 through 7) decreased *RSS* (as compared with Mix 2). It shall be noted that although the increased FA replacement in the mixtures only made small changes in the particle size distribution curve and *RSS* values, as shown in Figure 10 and Table 3, such small increases in packing may have contributed to the increase in 1-day compressive strength of Mixes 5 and 6 when compared to Mix 2 (see Table 2). Although having good particle packing, Mix 7 had much lower 1-day strength when compared to Mixes 5 and 6, probably due to the slow hydration of the larger amount of FA in the mix. As a result of the particle packing study, Mix 6 is considered as the final HPM.

3.3 Heat of Hydration and Setting Time

The rate of heat of hydration of the four mixtures were measured by isothermal calorimetry. The measurement gives information on the various exothermic reactions between the cementitious materials and water and the cementitious materials themselves. The heat generation process also reflects the characteristics of the tested materials and mixture proportions such as the onset of reaction, rate of reaction, and reactivity.

The first two mixtures selected for the isothermal calorimetry tests were the paste from the HPM (Mix 6 in Table 2 without river sand), with and without LF. The comparison of these two mixtures gives insight to the role of LF on HPM's hydration process. The effects of supplementary cementitious materials (SF and FA) on heat of hydration were not studied since they have already been well-documented (Ma et al. 1994, Wang et al. 2006). The third mixture was the paste from the C-3WR-C20, the proportion of which is given in Table 1, with the fine and coarse aggregates excluded. The result from the C-3WR-C20 serves as a base for comparison between the rapid repair mixes and conventional pavement concrete mix. The fourth mixture was the mortar sieved from the RSC (but note that the mortar was used in the test since the paste was unable to be obtained from this pre-packed commercial mix).

The calorimeter used was an 8-channel isothermal calorimeter manufactured by Thermometric Inc. Enclosed in a temperature control chamber, each channel measures heat flow from an individual sample independently. When a sample is placed in the calorimeter, the heat produced by the sample flows to the aluminum sample holder and towards a heat flow detector. The difference in heat detected between the sample sensor and the reference sensor created a voltage signal proportional to the heat flow. The voltage signal is then converted to the rate of heat evolution by applying a calibration factor. The calibration factor was obtained following the procedure described by Wang et al. (2007).

To perform the test for a given paste/mortar mix, 50 grams (g) of dry materials and the corresponding amount of water and admixtures were prepared for each measurement. The dry and liquid ingredients were placed in separate cups and placed in the calorimeter for 24 hours to condition them to the designed initial temperature (20°C). It is expected that after 24 hours, the temperature in the chamber should be 20°C and there shall be no heat flow from the samples in the chambers. After the conditioning, the dry and liquid samples were taken from the calorimeter, mixed, and placed quickly back into the calorimeter. Data from the sample heat generation was then recorded for at least 48 hours. The rate of heat generation in mW per gram of cement (mW/g) was calculated using the following equation: where R is the calorimeter data reading in mV, B is the calibrated base line in mV, CF is the calibration factor in mW/mV ranged between 14.21 to 16.16 mW/mV, ws is the mass of sample in grams, c is the mass of cementitious materials in grams, and w is the mass of water in grams.

$$P = \frac{(R-B)CF}{ws \Big/ \left(1 + w \Big/ c\right)} \tag{3}$$

The plot of the rate of heat generation for each mixture tested is shown in Figure 11.

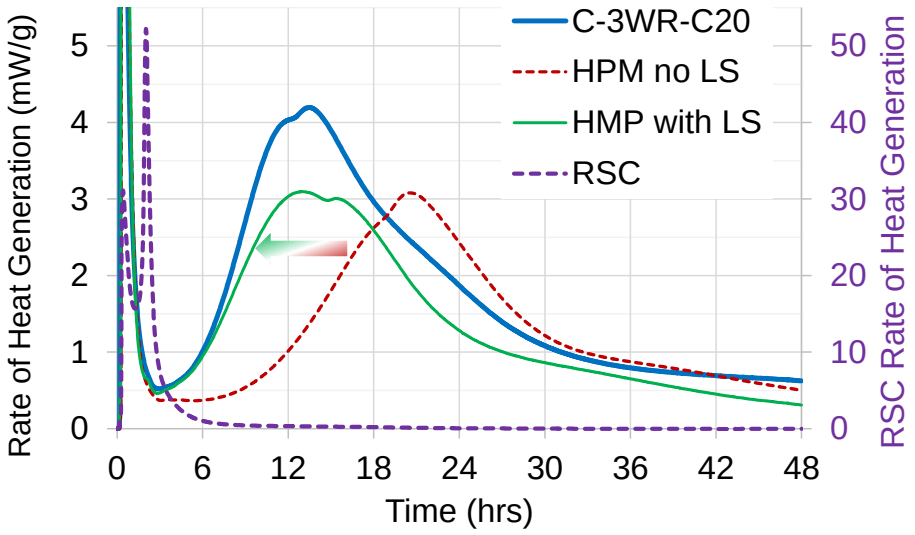

Figure 11. Rate of heat generation of pastes from rapid repair materials in the HPM with and without limestone fines, RSC, and conventional concrete C-3WR-C20 at 20°C

The peak rate of heat generated by the HPM is seen to be lower than the C-3WR-C20. This is likely due to the lower w/b ratio (RILEM 42-CEA 1981, Byfors 1980) and slightly higher percentage of supplementary cementitious materials. Paste with a higher w/b ratio has greater microstructural space and a larger amount of water available for hydration, thereby facilitating heat generation of hydration. It can also be seen in Figure 11 that the addition of LS into HPM reduces the time to reach the peak rate of heat generation. Research has shown that fine LS can have a nucleating effect on the hydration process and can also react with FA, thus increasing the rate of hydration (Bentz, et al. 2015). This demonstrates that the use of LS is beneficial to the development of a rapid repair material. For the mortar sample sieved for the RSC, the rate of heat generation can be described as a surge, which is 10 times higher than that of the C-3WR-C20 or HPM at a very early age and with a very short duration. The first peak rate of heat generation of the RSC is at 25 minutes after mixing, and the second and higher peak occurs at 120 minutes. This coincides with the rapid setting and strength gain of RSC, which sets at about 25 minutes after mixing.

Set times of the HPM, RSC, and C-3WR-C20 were measured according to ASTM C403. Samples tested were mortars sieved from freshly mixed concrete using a #4 mesh size sieve. The mortar samples were then placed in a cylindrical vessel and covered with a wet cloth between readings. Penetration readings were taken in given time intervals until the final set was reached. The initial setting (IS) time is the time when the penetration resistance of the tested sample equals 500 psi, and the final setting (FS) time is the time when the resistance reaches 4,000 psi. The test results are given in Figure 12.

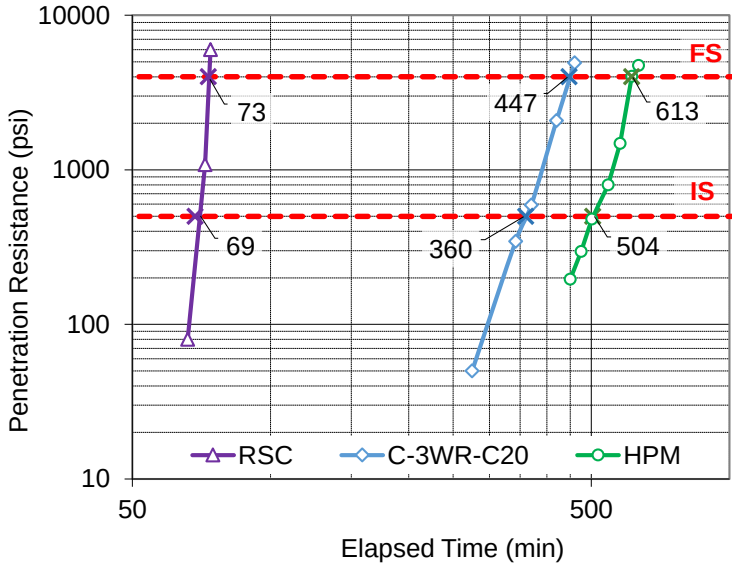

Figure 12. Penetration resistance of the HPM, RSC, and C-3WR-C20, indicating initial set time (IS = 500 psi) and final set time (FS = 4,000 psi)

As seen in Figure 12, the order of set time, form fast to slow, of the tested samples is the RSC, C-3WR-C20, and HPM. The IS and FS times were 504 and 613 minutes (8.40 and 10.22 hours), respectively, for the HPM, while for the C-3WR-C20 the times were 360 and 447 minutes (6.00 and 7.45 hours). That is, there was about a 2.5 hour delay in set times for the HPM when compared with the C-3WR-C20. The interval between the FS and IS times was 109 minutes for the HPM and 84 minutes for the C-3WR-C20. For the RSC, the IS and FS times are 69 and 73 minutes (1.15 and 1.22 hours), respectively, which was about 5 to 6 hours earlier than those of the C-3WR-C20. It can also be observed that the IS and FS times for the RSC are only 4 minutes apart. If it is rounded off to the nearest 5 minute mark, as specified in ASTM C403, such a difference (of 4 minutes) would not be sufficient to distinguish between IS and FS. It should be noted that RSC was designed to be ready for traffic loads in 1 hour.

4 MECHANICAL PROPERTIES

4.1 Compressive Strength and Elastic Modulus

The compressive strength development and elastic modulus in compression of the HPM, RSC, and C-3WR-C20 were measured following AASHTO T 22 (ASTM C38) and ASTM C469, respectively. The strength development determines the ability of the new mix to timely gain the needed strength and rigidity for immediate service. Three cylinder samples were prepared for each testing day. The samples tested were 4 in. (diameter) × 8 in. (height) cylinders. The test days were 1, 3, 7, and 28 days after casting. The samples were stored in a moist curing room until testing. Also tested was a variation of the HPM, where microfibers were added in the mixture. This mixture type was designated as HPM-f. The amount of microfibers added was 70 pcy.

Figure 13 and Figure 14 show the compressive strength and elastic modulus of the mixes.

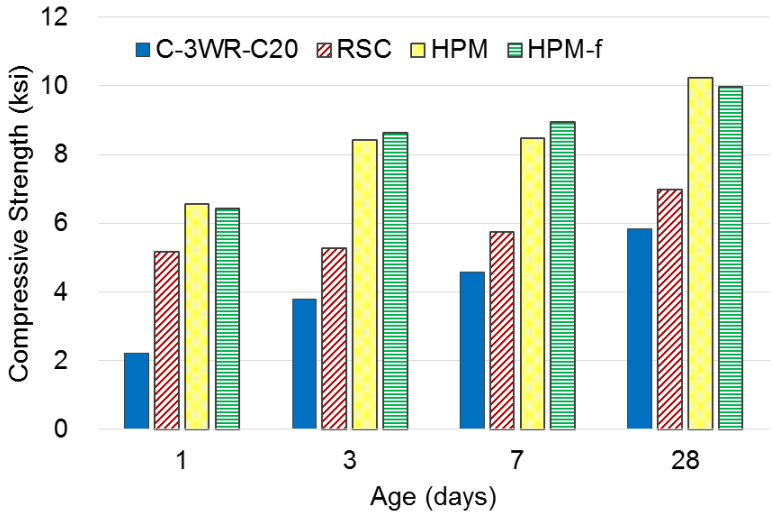

Figure 13. Compressive strengths of the HPM without and with steel fibers, RSC, and C-3WR-C20 at 1, 3, 7, and 28 days

As can been seen in Figure 13, the order of compressive strength of the tested mixes, from low to high, was the C-3WR-C20, RSC, and HPM/HPM-f, at all ages tested. The compressive strength of the HPM/HPM-f mixes exceeded 6,000 psi at 1 day, which was approximately 25 percent higher than that of the RSC. For the rest of testing ages (up to 28 days), the compressive strength of the HPM/HPM-f mixes was about 30 percent higher than that of the RSC. At 28 days, the HPM/HPM-f reached 10,000 psi, while the RSC was at about 7,000 psi. These test results suggest that although there was some delay in set time, the HPM/HPM-f mixes had sufficient strength development, which meets the requirement for rapid pavement repair.

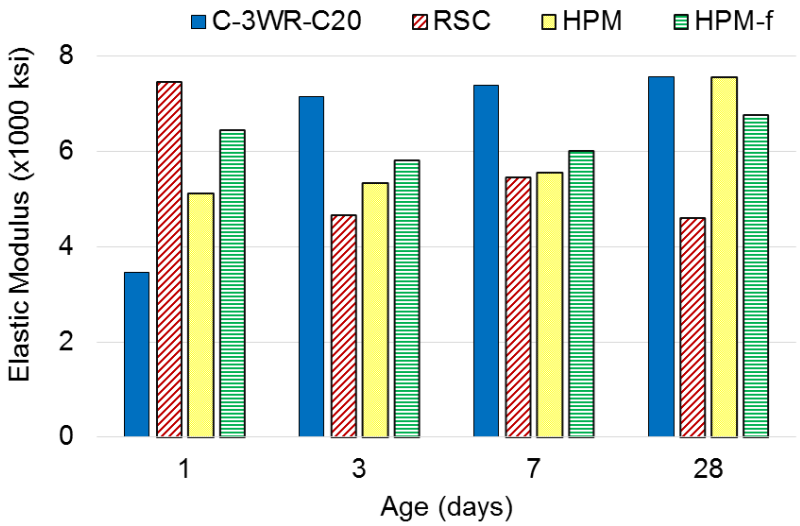

Figure 14. Elastic modulus of the HPM, HPM-f, RSC, and C-3WR-C20 at 1, 3, 7, and 28 days

Figure 14 shows that the elastic modulus of the HPM was higher than that of the C-3WR-C20 at 1 day, lower than that of the C-3WR-C20 at days 3 and 7, but comparable to that of the C-3WR-C20 at 28 days. The elastic modulus of the HPM-f began high and maintained its value until the 28th day. The elastic modulus of the RSC was much higher than that of the C-3WR-C20 at 1 day, but it quickly decreased and became much lower than that of the C-3WR-C20 at 28 days. These results suggest that used as a repair material for substrate concrete C-3WR-C20, the HPM/HPM-f is much better in compatibility than the RSC. The reduction of an elastic modulus in the RSC may be due to an extended period of saturation that occurs during curing.

4.2 Modulus of Rupture

Most unreinforced concrete members depend on rupture or flexural strength to sustain imposed loads. For unreinforced pavements in particular, loads landing near the edge or corner of slabs impose rupture stresses at the top section. The modulus of rupture at the different ages of the HPM, HPM-f, RSC, and C-3WR-C20 were measured using AASHTO T 97 (ASTM C78) or simple beams with third-point loading. The beams prepared for the tests were 3×3×11 in. and were kept under moist curing until testing. The tests were conducted at 1, 3, 7, and 28 days after casting.

The different moduli of rupture for the tested beams are given in Figure 15.

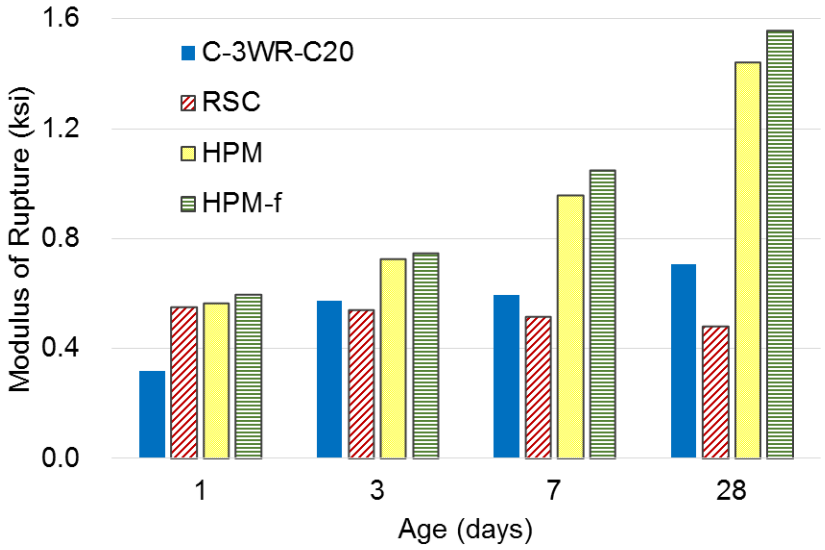

Figure 15. Modulus of rupture of the HPM without and with steel fibers, RSC, and C-3WR-C20 at 1, 3, 7, and 28 days

The modulus of rupture of the HPM was similar to that of the RSC at 1 day. The modulus of rupture for the HPM continuously increased with time, up to twice that of the C-3WR-C20 at 28 days. The RSC, on the other hand, had a modulus of rupture value of about 40 percent higher than that of the C-3WR-C20 at 1 day but about 30 percent lower than the C-3WR-C20 at 28 days due to a slight decreasing trend with time. The modulus of rupture of the HPM-f is consistently higher than that of the HPM due to the presence of steel microfibers. Based on the modulus of rupture and compressive strength test results at 28 days, the HPM is also a potential repair material for higher strength concrete.

4.3 Slant Shear Strength

One of the important mechanical properties of a patch repair material is its ability to adhere to an existing concrete. A good bond between the repair material and the existing concrete facilitates restoration of load carrying capacity and performance. The most common test method for measuring bond strength for repair materials is ASTM C882. This test measures the shear strength of a bond between materials by applying a compression load on cylinder samples, thereby not requiring special equipment for the test.

The samples for this test were composed of two components: the substrate and the repair material (as shown in Figure 16).

Figure 16. Slant shear sample composed of sandblasted substrate (left) and substrate (lighter color) and patch material combined as a 4 by 8 in. sample (right)

The substrate used in the present study was made using the C-3WR-C20. It was first cast as a whole 4 by 8 in. (height) cylinder. The cylinder were cured moist for 28 days and was then cut diagonally to conform to the dimension requirements of ASTM C882. The cut samples were then sandblasted until a difference between the limestone aggregates and the mortar on the surface of the sample was distinguished. To cast the repair material on the substrate, the cylinder halves were placed in a 4 by 8 in. cylinder mold and were pre-wetted with a wet towel. Freshly mixed repair materials were then cast on the substrate. The RSC repaired samples were vibrated on a vibrating table for 10 seconds, while the HPM repaired samples were only tapped on the sides of the cylinder to ensure sufficient filling inside the mold since the HPM is self-consolidating. The repaired cylinders were removed from the mold after 24 hours and placed under moist curing until tested.

The results of the slant shear strength tests are shown in Figure 17.

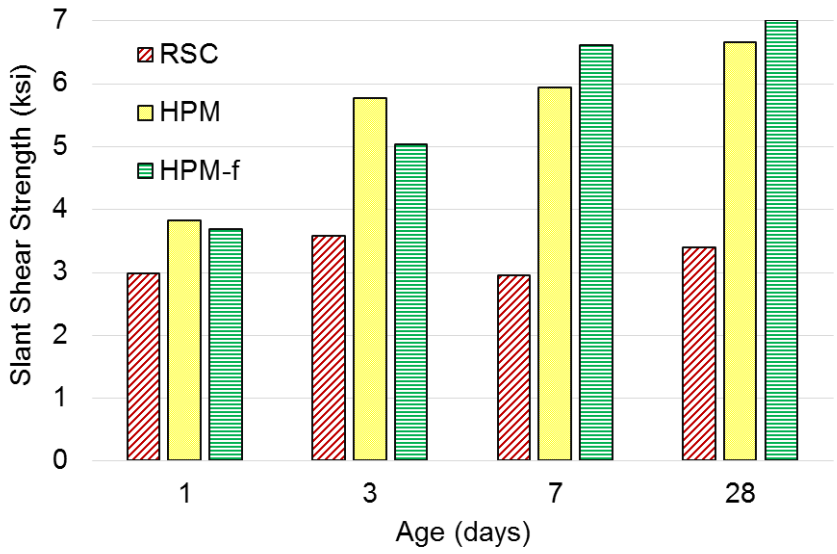

Figure 17. Slant shear strength of HPM without and with steel fibers and RSC at 1, 3, 7, and 28 days

One day after casting, the slant shear strength of the HPM, HPM-f, and RSC were 3,817, 3,680, and 2,971 psi, respectively. The mode of failure was all at the interface (i.e. a bond shear failure). At 3 days and later, the slant shear strength of the HPM and HPM-f was greater than 5,000 psi and continuously increased with time. During this time period, the failure of the substrate governed the strength of the HPM and HPM-f samples. Differently, the slant shear strength of the RSC didn't go beyond 3,573 psi during the 28-day testing period, and the sample continuously failed at the patch-substrate interface, which indicated a weak bond (see Figure 18).

Figure 18. Typical slant shear failure modes: bond interface failure with the two halves separating at the interface (left) and substrate failure where the substrate cracks and breaks (right)

4.4 Direct Pull-off Strength

The direct pull-off strength test follows ASTM C1583. Different from slant shear strength, the direct pull-off strength test measures the tensile capacity of the bond between the substrate and the patch material. This type of failure may occur at the tension side of a bending deformation. In the tensile loading case, the contribution surface roughness interlocking between the substrate and patch into strength is diminished. What is measured is how strong the two materials adhere to each other.

Two types of substrates were prepared for the test: the C-3WR-C20 and O-4WR. The 6×6×21 in. molds were prepared by first placing a 2×6×21 in. polystyrene foam board at the bottom of the mold. This left a 4 in. thick space to form the substrate. The sides of the mold and the polystyrene were oiled and filled with concrete. The concretes were consolidated with an internal vibrator. The top surface was troweled and covered with a plastic sheet and a wet cloth until demolding. The slabs were demolded after 24 hours and were placed under moist curing for 28 days. At the end of moist curing, one side of the slabs was sandblasted in the same procedure as the slant shear substrates, as shown in Figure 19.

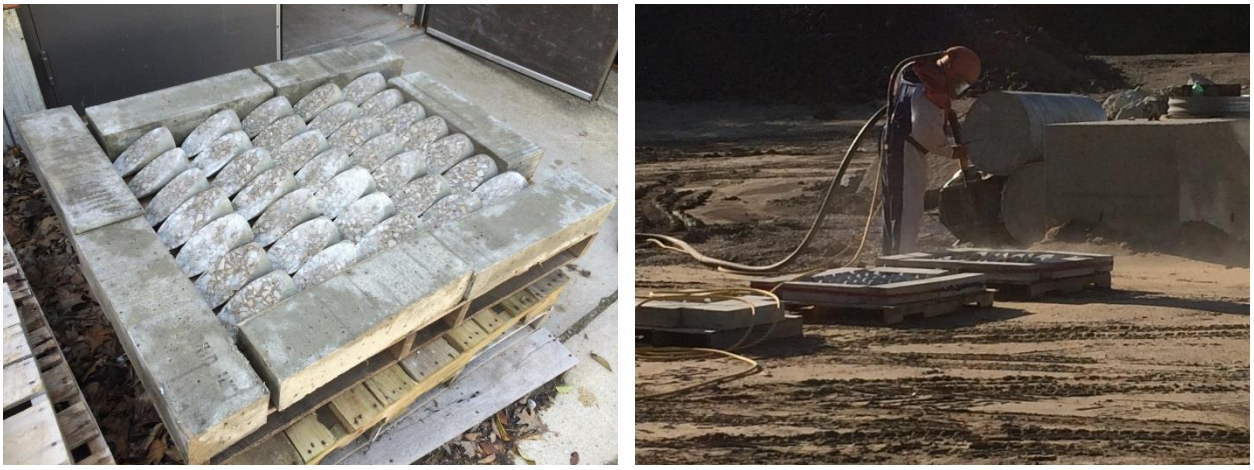

Figure 19. Sandblasting of samples for bond test: slant shear substrates on a pallet that is bordered with 4×6×21 in. substrate slabs (left) and actual sandblasting of substrates (right)

The sandblasted and troweled/without sandblasting surfaces of a slab are shown in Figure 20.

Figure 20. Slab surfaces: sandblasted surface (left) and troweled surface without sandblasting (right)

The substrate slabs were placed inside the 6×6×21 in. molds. Since the slabs are only 4 in. thick, there was a 2 in. space for casting rapid repair mixtures. Before casting the rapid repair mixtures, the substrate surface was moistened. The mixtures of HPM, HPM-f, and RSC were mixed and placed on the substrates. Before the mixtures were placed, the substrates were either grouted or not grouted. Grouting is the process by which a stiff brush is dipped in a rapid repair mixture and brushed on the substrate. After placement, the freshly placed mixtures were covered with a plastic sheet and wet cloth until demolded. The slabs were demolded 16 hours after casting. The patch and substrate were cut with a 2 in. core drill bit, to be able to conduct the pull-off tests. The drill bit went through the depth of the patch and 1 in. into the substrate, as shown in Figure 21.

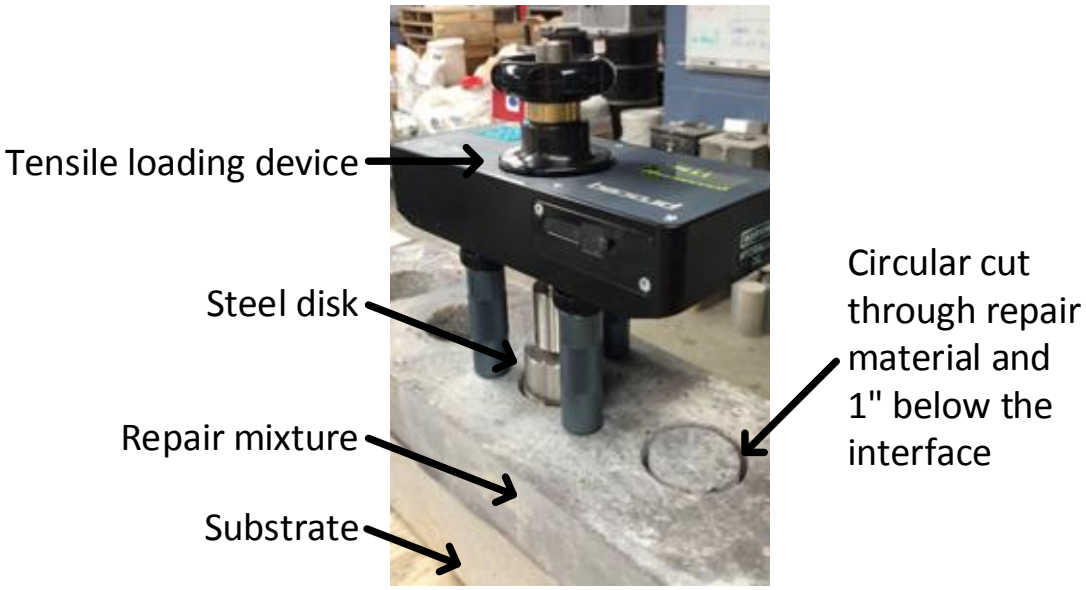

Figure 21. Direct pull-off test with loading device (Proceq DY-2 model) mounted on sample slab

Four circular cuts were made on each slab. The first cut was made after demolding, while the remaining cuts were made on the third day. Two samples were made for the test. When the slabs were not being tested, they were placed in moist curing.

On the day of direct pull-off testing, the steel disk and loading device were mounted on the rapid repair mixture, as previously shown in in Figure 21. The procedure for mounting and testing is listed as follows:

1. Remove water on the patch surface and in the circular cut. Lay the sample on its side and blow the surface and the inside of the circular cut with pressurized air.

2. Scrub the surface of the cylinder (concrete bound by the circular cut) with a steel brush to remove any loose materials and roughen the surface. Blow the surface with pressurized air to remove debris.

3. Ensure that the bottom of the steel disk that will be facing the rapid repair mixture is clean. Epoxy (or cylinder) from previous tests may be removed by heating the steel disk on a hot plate and scraping the epoxy using a steel spatula. Use proper protective clothing and equipment when handling the heated steel disk. Use sand paper to remove any remaining small fragments that cannot be removed using a steel spatula.

4. Mix the two-part epoxy and apply a film on both the patch surface and the steel disk.

5. Place the steel disk on the patch material. Ensure that there are no gaps between the steel disk, epoxy, and the patch material. Do not let any excess epoxy flow down the circular cut. Scrape excess epoxy using a craft stick.

6. Cure the epoxy in room temperature for at least 6 hours before loading. Mount the loading device and load at a rate of 5 psi. Record the failure load and the failure mode. The different failure modes, as described in ASTM C1583, are shown in Figure 22.

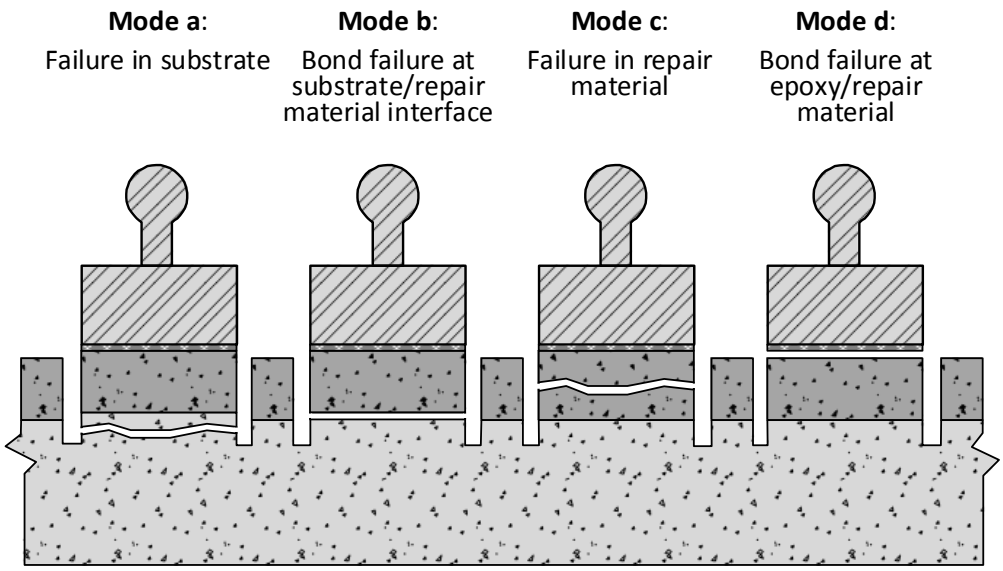

Figure 22. Failure modes

It is important to mount the steel disk in a secure and timely manner. Most epoxies require a curing period of 24 hours, even with a short (5 minute) setting time. After testing several types of epoxies, it was found that a repair and anchoring epoxy (i.e., PC-Concrete) provided timely strength gain for 1-day testing of the bond. The pull-off bond strength of the epoxy was tested by bonding the steel disk to concrete. A cut with a core drill bit was not made to increase the chance of epoxy failure, as shown in Figure 23, as opposed to concrete tensile failure.

Figure 23. Testing of epoxy: steel disk epoxied to an uncut concrete surface (left), epoxy failure after direct-pull off test (center), and concrete failure due to good epoxy bond (right)

4.4.1 Pull-off Strength between Repair Materials and C-3WR-C20 Substrates

The pull-off strengths for rapid repair mixtures, where the substrates were not grouted, are given in Figure 24.

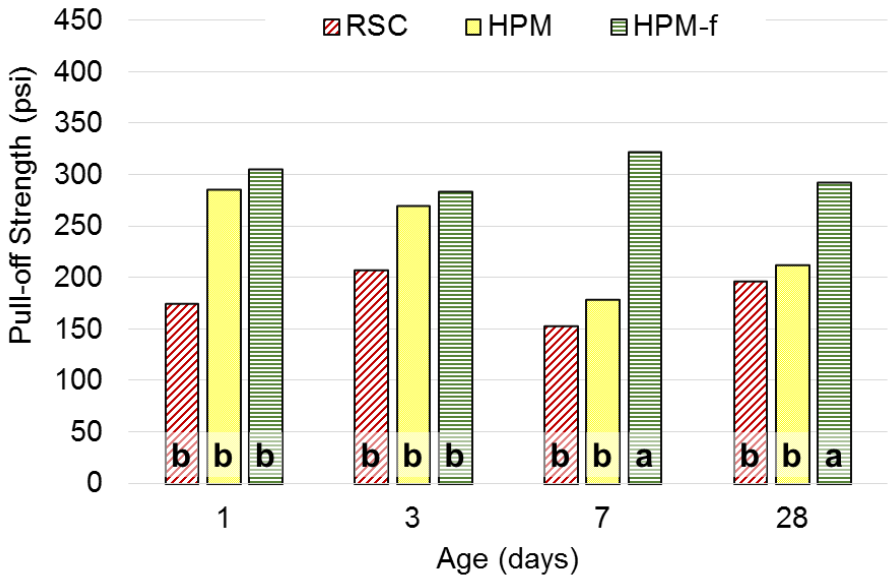

Figure 24. Pull-off strength of rapid repair mixtures with sandblasted but not grouted C-3WR-C20 substrates where (a) shows substrate failure and (b) shows bond failure

The mode of failure is noted by the letters in the graph bars. The letters are defined in Figure 22. The pull-off strength of the HPM was much greater than the RSC at 1 day after casting. However, the pull-off strength of the HPM decreased over time. It is not clear why decreased pull-off strength of the HPM and RSC samples was observed and might be related to the balance between the shrinkage of the repair materials and bond strength development. Although decreasing with time, the pull-off strength of the HPM samples were always higher than that of the RSC samples. Moreover, the pull-off strength of the HPM-f at 1 day was similar to that of HPM at 1 day and was maintained during the testing period (up to 28 days). Since the only difference between the HPM and HPM-f was the presence of steel fibers in the HPM-f, this implied that shrinkage of the HPM caused a reduction in the bond/pull-off strength. As discussed later, the HPM-f had a reduced amount of shrinkage compared to the HPM.

The results of the HPM and RSC pull-off test with substrate grouting are shown in Figure 25.

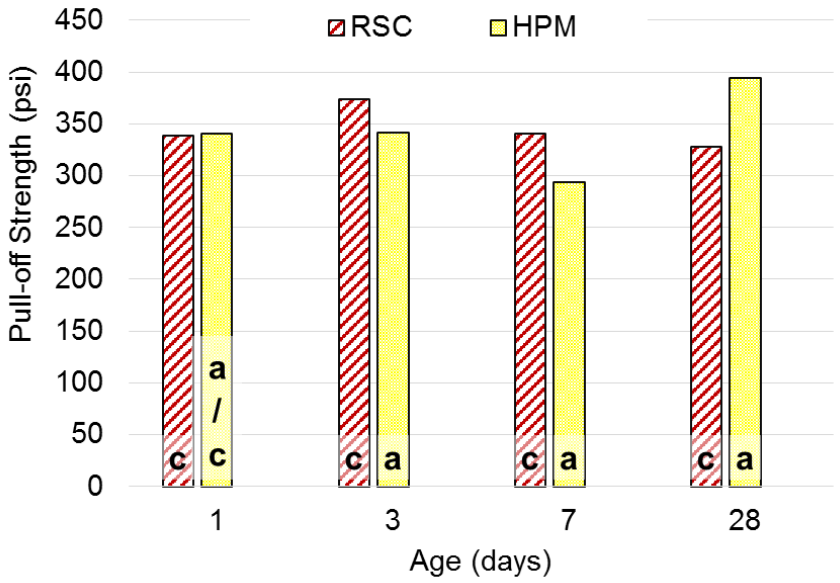

Figure 25. Pull-off strength of rapid repair mixtures with sandblasted and grouted C-3WR-C20 substrates where (a) shows substrate failure and (c) shows repair material failure

It can be observed that with grouting, the bond between the rapid repair materials and the substrate was stronger; therefore, higher pull-off strengths were obtained from the samples with grouting compared to the samples without grouting. During grouting, the repair material was scrubbed into the substrate and permeated into the substrate and filled surface pores and voids, thus providing a better bond between the repair material and the substrate. Therefore, bond failure was no longer observed, and the decrease in the pull-off strength was minimized. Based on the mode of failures observed, tensile failure was initiated at the repair material when the RSC was used for repair, whereas the C-3WR-C20 substrate fracture governed the failure when the HPM was used for repair.

4.4.2 Pull-off Strength between Repair Materials and O-4WR Substrates

The pull-off strength of the HPM with a high-performance concrete and O-4WR as a substrate was also tested. Three types of substrate surface preparations were investigated: sandblasted and grouted, sandblasted but not grouted, and not sandblasted and not grouted. The results of the pull-off strength tests are given in Figure 26.

Figure 26. Pull-off strength of rapid repair mixtures with O-4WR substrates showing (a) substrate failure and (b) bond failure

It can be observed that the pull-off strength values between the repair materials studied and O-4WR substrate were all higher than those between the corresponding repair materials and C-3WR-C20 substrate at a given testing age.

The sandblasted and grouted samples provided the highest pull-off strengths. Sandblasting made a high surface roughness, and grouting pushed the rapid repair material into the rough dens, which created a strong grip between the two materials. It can be noted that bond failure occurred at 1 day. In this case, the substrate was stronger than the rapid repair material. At 3 and 7 days, the failures were observed at the bond or at the substrate. During this time, the strengths of the HPM and strength of the substrate were similar. At 28 days, the failure occurred completely at the substrate, since the HPM was stronger than the substrate.

The lowest pull-off strength was obtained from substrates without sandblasting and grouting, where the surface pits and voids were shallower. Without grouting, the amount of material that could interpenetrate at the interface was also less. However, the pull-off strength at 28 days without sandblasting and without grouting increased to the level of with sandblasting and grouting. At the early ages of 1, 3, and 7 days, bond failures were observed, but at 28 days, substrate failures were observed. This implies that with sufficient curing, a strong bond was developed between the HPM and the substrate. Although the bond strength was low at the early age, the samples without sandblasting also developed sufficient bond strength over the curing period.

The pull-off strength with a sandblasted but not grouted surface was in the intermediate of the pull-off strengths. The sandblasted surface increased the surface area and roughness, but without grouting the possible contacts on the surface were not fully utilized.

5 DURABILITY PROPERTIES

5.1 Cyclic Freezing and Thawing

The durability of the HPM, HPM-f, RSC, and C-3WR-C20 to cyclic F-T was measured according to ASTM C666, Method B. Two 3×4×16 in. prisms were prepared for each mix. Of the four mixes, only the C-3WR-C20 was air entrained. The RSC was prepared by simply mixing the pre-packed mixture with water. The HPM and HPM-f were intentionally mixed without adding air entraining admixture. The prisms were moist cured for 28 days before being subjected to F-T cycles. The tests were conducted until 300 cycles were reached. The durability factor, mass loss, and pictures of the prisms after the test are shown in Figure 27, Figure 28, and Figure 29, respectively.

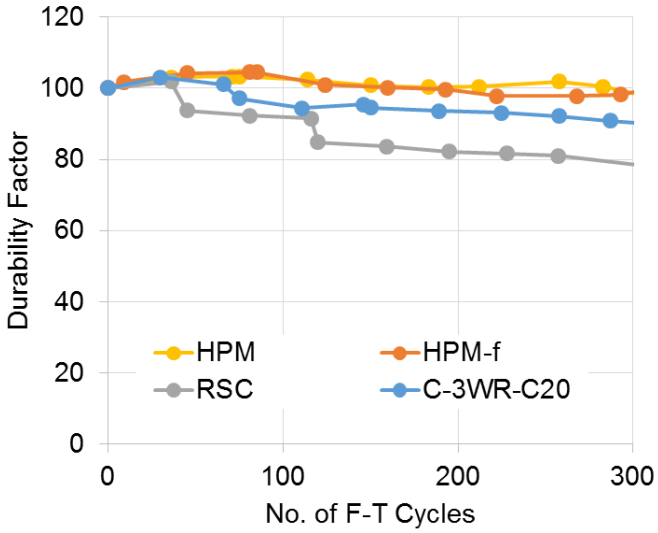

Figure 27. Durability factor of concrete prisms under cyclic F-T test

It can be seen from Figure 27, the HPM and HPM-f mixes are F-T durable, even without air entrainment. There was no significant change in relative dynamic modulus measured for the prisms made with the HPM and HPM-f mixes. However, the durability factor of the C-3WR-C20 reduced to 90 percent, while on the other hand the RSC reduced to 80 percent after 300 F-T cycles.

Similarly, Figure 28 shows that there was little/no change in mass for the HPM and HPM-f mixes, but there was a slight reduction in mass for the C-3WR-C20 mix and a much greater reduction in mass for the RSC.

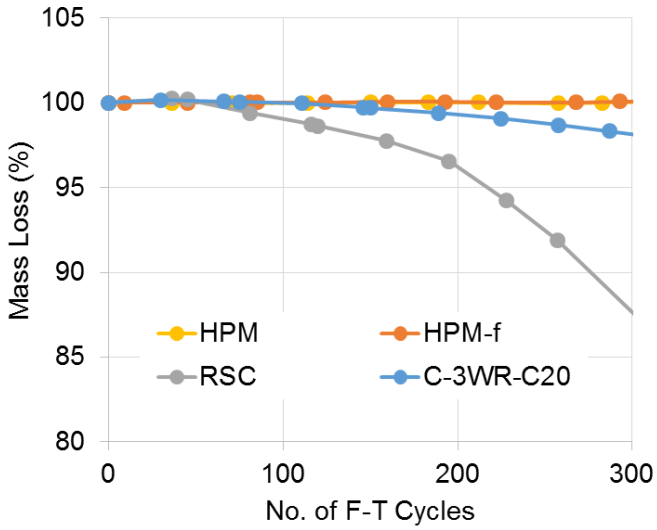

Figure 28. Percent mass loss of concrete prisms under cyclic F-T test

The mass reduction can be visually evaluated in Figure 29, and the loss in mass from the RSC is significant.

Figure 29. Prisms after 300 F-T cycles: HPM (upper left), HPM-f (upper right), RSC (lower left), and C-3WR-C20 (lower right)

The results indicate that the F-T deterioration of concrete repaired using the HPM and HPM-f mixes would not initiate from the rapid repair material. On the other hand, if F-T durable concrete is patched with the RSC, the repaired concrete would be susceptible to F-T deterioration and would likely be needing re-repair on the same area as the patch.

5.2 Shrinkage

Shrinkage of a repair material often causes the failure of the bond between the substrate and repaired concrete, as substrates are commonly matured and do not shrink further. Therefore, the amount of shrinkage of the rapid repair materials was measured in the present study. Two types of shrinkage were measured for the HPM, HPM-f, RSC, and C-3WR-C20: autogenous shrinkage and free (unrestrained) drying shrinkage. The autogenous shrinkage was measured following ASTM C1698. The autogenous shrinkage device requires the use of corrugated plastic tubes (see Figure 30).

Figure 30. Corrugated plastic tubes used in autogenous shrinkage device

The tube diameter opening was between 0.83 and 0.88 in. In order to fill the corrugated plastic tube with the RSC and C-3WR-C20 mixtures, the course aggregates in these mixtures were removed from freshly mixed concrete with a #4 sieve. The HPM and HPM-f mixtures do not have large aggregates and were able to completely flow though the tube opening. While filling, the tube was placed on a vibrating table to ensure that bubbles were expelled. After filling and sealing the tubes, the first measurements were taken at the final setting times, which are given in Figure 12. Subsequent measurements were taken at 1, 3, 7, 14, 28, and 56 days after casting. The results of the autogenous shrinkage measurements are shown in Figure 31.

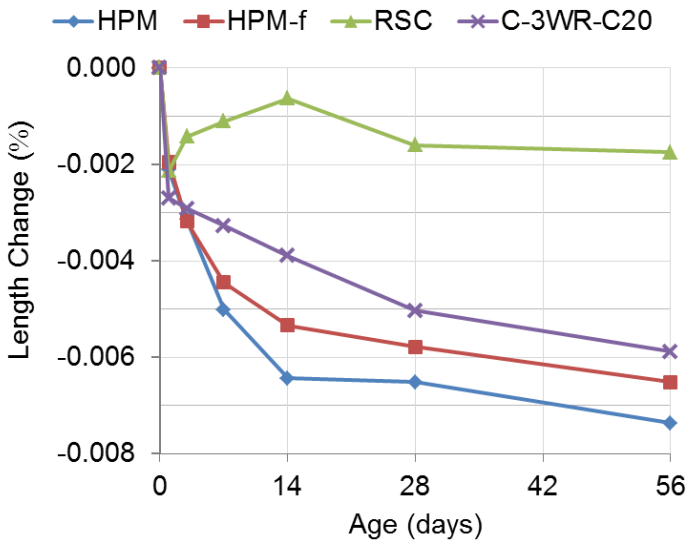

Figure 31. Length change due to autogenous shrinkage of the HPM, HPM-f, RSC, and C-3WR-C20

The results showed that the HPM had higher autogenous shrinkage than the C-3WR-C20 during its first early age, while autogenous shrinkage of the RSC was minimal. The addition of fibers reduced the amount of autogenous shrinkage. It should be noted that the binder for the RSC was calcium sulfoaluminate while the binder for the HPM and C-3WR-C20 was predominantly portland cement. The high autogenous shrinkage of the HPM resulted from the continued hydration of portland cement at a very low w/b (0.25), which resulted in self-desiccation in the system.

The free drying shrinkages of the HPM, HPM-f, RSC, and C-3WR-C20 were measured following ASTM C157. Three prisms of 3×3×11 in. were made for each mixture type. The prism gage length was 10 in. The mixtures were kept in their molds for 1 day before demolding. After demolding, the prisms' initial length comparator reading and weight were recorded. The prisms were then placed in a moist curing room for 27 days. After 27 days, the prisms' surfaces were dried and length and weight measurements were taken. The prisms were then stored in a drying room, as shown in Figure 32, at a temperature of 73±3°F with relative humidity of 50±4% for subsequent measurements. Additional length and weight measurements were obtained at 3, 7, 14, 28, and 56 days.

Figure 32. Drying shrinkage samples

The calculated percent change in length and weight were presented in two ways: the changes due to drying only and the changes due to moist curing and drying, which showed the swelling behavior of the mixes during moist curing or wetting. Figure 33 and Figure 34 show the percent length and weight changes during drying.

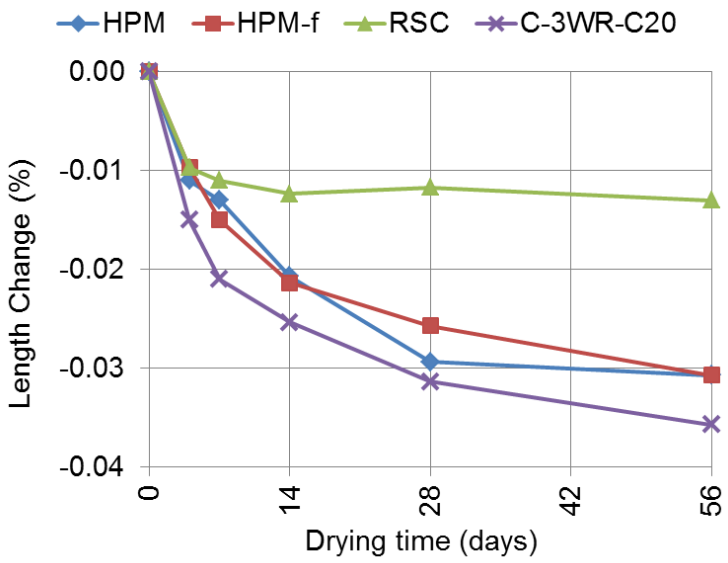

Figure 33. Length change due to free drying shrinkage of the HPM, HPM-f, RSC, and C-3WR-C20

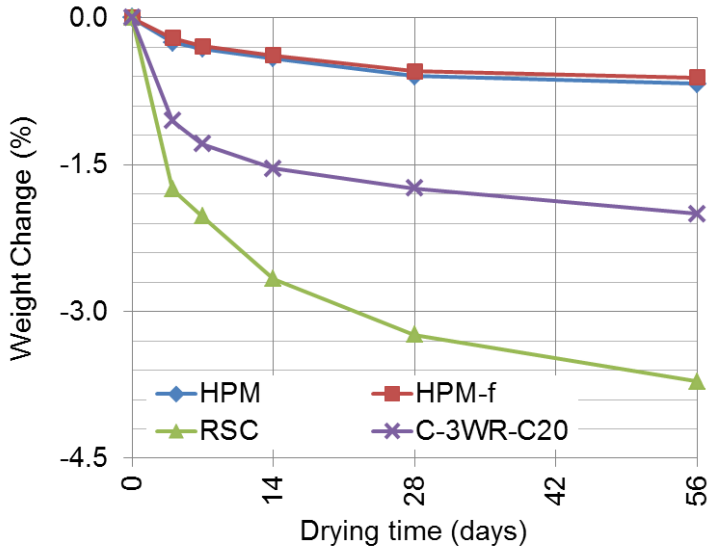

Figure 34. Weight change due to drying of the HPM, HPM-f, RSC, and C-3WR-C20

Figure 35 and Figure 36 shows the total length and weight changes that include the moist curing period and the drying period, respectively. All percentage calculations are based on the length and weight obtained immediately after demolding.

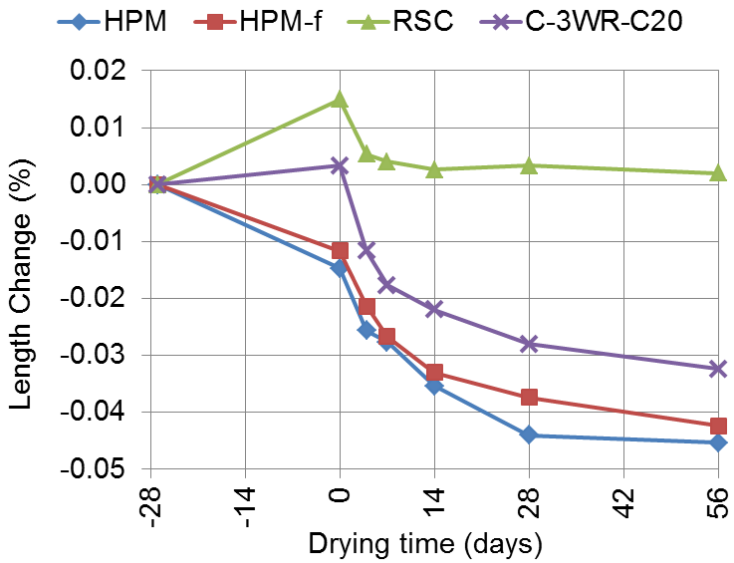

Figure 35. Total change in length change due to moist curing followed by free drying shrinkage of the HPM, HPM-f, RSC, and C-3WR-C20

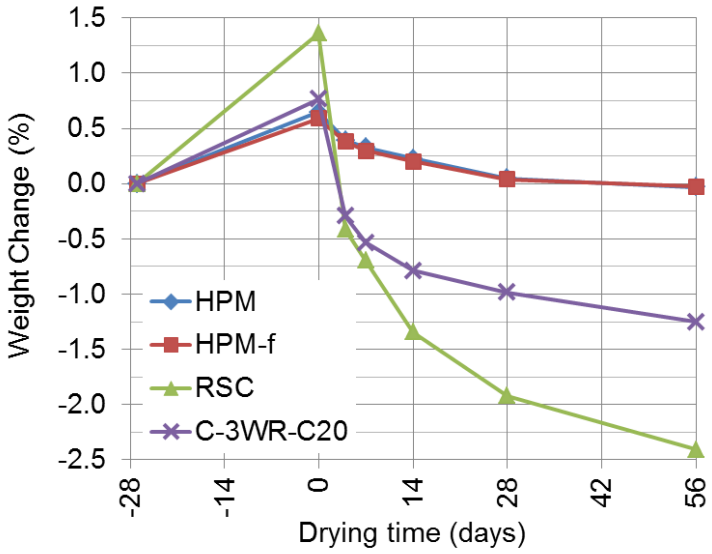

Figure 36. Total weight change due to moist curing and drying of the HPM, HPM-f, RSC, and C-3WR-C20

The following can be observed from Figures 33 through 36:

- The RSC, consisting of calcium sulfoaluminate cement as a binder, showed significant extension/swelling and weight gain during moist curing, followed by the C-3WR-C20, while the HPM and HPM-f showed substantial shrinkage and a little weight gain during moist curing (see Figures 34 and 36).

- Among all the mixes tested, the RSC had the lowest free drying shrinkage (see Figure 33) but the highest weight loss (see Figure 35) during drying. One possibility is that the RSC might have a high porosity, which allowed water to easily move in and out, thus resulting in a small effect on volume change. Further study on this commercial repair material is needed.

- The HPM and HPM-f had a much higher drying shrinkage than the RSC but less drying shrinkage than the C-3WR-C20 (see Figure 33). Different from those in autogenous shrinkage, fibers in the HPM-f had little effect on the free drying shrinkage of the HPM.

- As seen in Figure 36, the weight gain of the samples made with the HPM and HPM-f during moist curing was the lowest among the four mixes tested, which was a result of the amount of water absorbed. Since the water absorbed by a sample during moist curing could serve as a water supplier to reduce self-desiccation or autogenous shrinkage of the sample, this result suggests that the HPM and HPM-f mixes had a high potential for extensive self-desiccation and high autogenous shrinkage, which is consistent with the result observed in Figure 31.

- Figure 36 also shows that about the same amount of water absorbed by the HPM and HPM-f mixtures had evaporated during drying. Although the amount of water loss was small, the

mixes had an intermediate value of drying shrinkage, which was probably related to their fine pore structure provided by a low w/b (0.25) of the mixes.

- The C-3WR-C20, which had lower portland cement content, higher w/b, and higher coarse aggregate content than the HPM, displayed a noticeably higher drying shrinkage and a much higher weight loss during drying. It shall be noted that although the weight loss, resulting from water evaporation, of the C-3WR-C20 was much higher than that of the HPM, the drying shrinkage value of the C-3WR-C20 was only a little higher than that of the HPM. This once again indicates that it is not the amount of water evaporated but the pore structure of the concrete materials that primarily controls the degree of their shrinkage. Therefore, further study shall be conducted on the pore structure of the materials.

- The order of the total shrinkage (autogenous and free drying shrinkage) of the mixes studied, from lowest to highest, was RSC, C-3WR-C20, HPM-f, and HPM.

5.3 Permeability

Two types of permeability measurements were conducted. The first test was the rapid chloride permeability (RCP) test, which determined the electrical conductance of a sample to provide an indication of its resistance to the penetration of chloride ions, according to ASTM C1202. The RCP test samples included 4×8 in. cylinders that were moist cured for 28 days. The cylinders were cut into 2 in. disks and were vacuum saturated and mounted on test cells, based on ASTM C1202. Three disks from three cylinders were tested for each mixture type. The HPM-f was not tested due to the presence of micro-steel fibers, which are conductive.

The second test was a surface resistivity (SR) test (ASTM WK37880), which is considered as an alternative to the RCP test. The device for measuring the surface resistivity is a Wenner 4-electrode probe with 1.5 in. spacing. The samples were 4×8 in. cylinders. The samples were moist cured for 28 days after casting, when the samples were tested. The samples were wiped with a cloth to make the surface saturated surface dry prior to testing. The samples for RCP and SR were the same samples. The results of the tests are listed in Table 4.

Table 4. Rapid chloride permeability and surface resistivity of substrate and rapid repair mixtures

	Rapid Chloride Permeability		**Surface Resistivity**	
	Charge Passed (coulombs)	**Class**	**Resistivity (kΩ-cm)**	**Class**
HPM	18	Negligible	222	Negligible
RSC	2,550	Moderate	21	Moderate
C-3WR-C20	1,829	Low	17	Moderate

HPM has a very low charge passed and very high surface resistivity. This is indicative of very low permeability. This would be consistent with the results of the cyclic F-T test: weight changes

during moist curing and drying. Even without air entrainment, the HPM was F-T durable because water was unable to sufficiently permeate into the samples to saturate it and cause deterioration by the stress from the expanding freezing water. This very low permeability may also explain the continued autogenous shrinkage of prisms even when under moist curing, as discussed in Section 5.2. The RSC had a slightly higher permeability compared to the C-3WR-C20. This explains its need for a proper entrained air void structure in order to be F-T durable. The C-3WR-C20 had an entrained air void system that made it F-T durable. Having a more permeable microstructure, the RSC is more susceptible to F-T damage compared to the C-3WR-C20, thus the RSC requires proper air entrainment.

6 CONCLUSIONS AND RECOMMENDATIONS

6.1 Conclusions

- A high-performance mortar can be achieved for rapid concrete repair using a high volume of industrial by-/co-products such as limestone fines, fly ash, and silica fume. The newly developed rapid repair HPM is highly workable, strong, and durable.

- Particle packing has a significant influence on the early age strength of the newly developed HPM, analyzed by the modified A&A model (Funk and Dinger 1994). In addition to their pozzolanic properties, proper silica fume and fly ash replacements for portland cement can help adjust particle packing and improve the workability and strength of the mortar. In addition to serving as fine aggregate or filler, limestone fines also accelerate hydration of cementitious materials in the HPM.

- The newly developed HPM possesses excellent self-consolidating ability: highly flowable, non-segregating, and no need for additional consolidation during casting.

- The compressive strength and modulus of rupture of the HPM at 1 day are comparable to the corresponding properties of conventional pavement concrete at 28 days. This suggests that the new rapid repair mixture is applicable for patch repair (requires compressive strength) and full-depth pavement repair (requires both compressive and flexural strength). As a comparison, the commonly used pavement repair material—RSC— is a commercially available, pre-packed concrete with a 1-day compressive strength comparable to the 28 compressive strength of the normal strength substrate (C-3WR-C20), but its modulus of rupture after 1 day is much lower than that of the C-3WR-C20.

- Sandblasted and grouted surfaces provides the best performance for bonding of a rapid repair material to a mature substrate. Differently, repaired concrete without sandblasting and/or grouting showed lower pull-off and slant shear strength in the present study. Slant shear strength values are generally higher than direct pull-off strength.

- The HPM is of excellent F-T durability, without the requirement for air entrainment. The F-T durability factor of the HPM stayed around 100 percent throughout the standard F-T test. Differently, the RSC showed significant mass loss during the F-T test, and its F-T reduced to about 80 percent at the end of the F-T durability test.

- The permeability of the HPM is extremely low (18 coulombs), which may contribute to its high F-T durability. Differently, the permeability of the RSC is much higher (2,550 coulombs).

- During moist curing, the HPM absorbed very little water and shrunk, while the RSC and C-3WR-C20 absorbed much more water and swelled. Under a sealed condition, the RSC

displayed little to no autogenous shrinkage, while the C-3WR-C20 displayed intermediate and the HPM displayed significantly high autogenous shrinkage. Under a drying condition, the RSC displayed low drying shrinkage, the HPM displayed much higher drying shrinkage, and was followed by the C-3WR-C20. As a result, the HPM had a higher total shrinkage than the C-3WR-C20, while the RSC had a small amount of total shrinkage. The addition of the micro-steel fibers (70 pcy) slightly reduced the shrinkage of the HPM.

- The set times of the HPM were about 2.5 hours longer that those of the C-3WR-C20. However, the delayed set times didn't affect the 1-day strength development of the HPM. Differently, the RSC set very quickly: 69 minutes for IS and 73 minutes for FS.

6.2 Recommendations

- The fatigue strength of a repair material can be investigated as a continuation of the research. When used for pavements, the repair (material and bond) will be subjected to repeated loading from vehicles. The repair material itself is likely to be able to withstand the fatigue stresses similar to a conventional pavement concrete. The critical component of the repair under repeated stress would be the interface between the two materials or the bond. With proper surface preparation and maturity, the bond under shear and tension was shown to be strong in the present study, but its performance under repeated loading is yet to be determined. When the interface between the repair material and the repaired concrete opens or de-bonds, the performance of the repaired structure reduces and harmful materials may accumulate at the opening and cause further deterioration. To investigate the properties of the repair material under repeated loading, a patch may be applied on the tension side of a beam and the beam subjected to repeated loads.

- Results from the present study have indicated that the pore structure of the concrete materials and not the amount of water evaporated primarily controls the materials' shrinkage behavior. Further study is needed on the pore structure of the repair materials. In addition, high shrinkage concrete does not always crack, depending upon other properties of the concrete such as elastic modulus, creep, and strength. Further study is necessary to investigate the cracking potential of the HPM. Since the total shrinkage of the HPM was higher than the total length change of the C-3WR-C20, methods of reducing the shrinkage such as shrinkage reducing admixture, shrinkage compensating admixture, and internal curing materials can also be explored. Optimal dosages of the admixtures may be determined. Upon reduction of shrinkage, the bond stress may be reduced and a better performance in the pull-off test may be obtained with and without grouting.

- Results of the RSC on F-T durability and RCP show poor or moderate performance. This opens the question for further investigation of other rapid repair material durability performance. Granting that repair materials need only to last as long as the remaining life of the concrete being repaired, durability of the rapid repair materials still needs to be known.

REFERENCES

Baron, J. and Douvre, C. 1987. Technical and Economic Aspects of the Use of Limestone Filler Additions in Cement. *World Cement*, 18(3): 100–104.

Bentz, D. P., Jones, S. Z., and Snyder, K. A. 2015. Design and Performance of Ternary Blend High-Volume Fly Ash Concretes of Moderate Slump. *Construction and Building Materials*, Vol. 84, pp. 409–415.

Bonavetti, V., Donza, H., Menendez, G., Cabrera, O., and Irassar, E. F. 2003. Limestone Filler Cement in Low W/C Concrete: A Rational Use of Energy. *Cement and Concrete Research*, 33(6): 865–871.

Byfors, J. 1980. *Plain Concrete at Early Ages*. Swedish Cement and Concrete Research Institute, Stockholm, Sweden.

Daimon, M. and Sakai, E. 1998. Limestone Powder Concerning Reaction and Rheology. Shigeyoshi Nagataki Symposium on Vision of Concrete: 21st Century, Tokushima, Japan, June 7-11, 1998. American Concrete Institute, Farmington Hills, MI. pp. 41–54.

Funk, J. E. and Dinger, D. 1994. *Predictive Process Control of Crowded Particulate Suspensions–Applied to Ceramic Manufacturing*. Springer Science+Business Media New York, NY.

Hornain, H., Marchand, J., Duhot, V., and Regourd, M. 1995. Diffusion of Chloride Ions in Limestone Filler. *Cement and Concrete Research*, Vol. 25, pp. 1667–1678.

Ma, W., Sample, D., Martin, R., and Brown, P. W. 1994. Calorimetric Study of Cement Blends Containing Fly Ash, Silica Fume, and Slag at Elevated Temperatures. *Cement, Concrete, and Aggregates*, 16(2): 93–99.

Moir G. and Kelham S. 1997. Developments in Manufacture and Use of Portland Limestone Cement, High-Performance Concrete: Design and Materials and Recent Advances in Concrete Technology. Proceedings of the Third CANMET/ACI International Conference, Kuala Lumpur, Malaysia, 1997. American Concrete Institute, Farmington Hills, MI. pp. 797–819.

Richard, P. and Cheyrezy, M. 1995. Composition of Reactive Powder Concretes. *Cement and Concrete Research*, 25(7): 1501–1511.

RILEM TC 42-CEA. 1981. Properties of Set Concrete at Early Ages: State of the Art Report. *Materials and Structures*, 14(84): 399–450.

Sato, T. and F. Diallo. 2010. Seeding Effect of Nano-CaCO3 on the Hydration of Tricalcium Silicate. *Transportation Research Record: Journal of the Transportation Research Board*, No. 2141, pp. 61–67.

Schmidt, M. and Fehling, E. 2005. *Ultra-High-Performance Concrete: Research, Development and Application in Europe*. American Concrete Institute, Farmington Hills, MI. pp. 51–78.

Schmidt, M., Fehling, E., Teichmann, T., Bunje, K., and Bornemann, R. 2003. Ultra-High Performance Concrete: Perspective for the Precast Concrete Industry. *Concrete Precasting Plant and Technology*, 69(3): 16–29.

TecEco Pty. Ltd. no date. Sustatinable Technologies. The Importance of Particle Packing for Strength, (Tec-Cements) or Carbonation (Eco-Cements). TecEco Pty. Ltd. Tasmania, Australia. www.tececo.com/technical.particle_packing.php#ftn11.

TRIP. 2012. *Key Facts about America's Surface Transportation System and Federal Funding*. The Road Information Program (TRIP), Washington, DC. Available at www.tripnet.org/docs/TRIP_National_Fact_Sheet_April_2012.pdf.

Walraven, J. C. 2002. From Design of Structures to Design of Materials: Innovations and Developments in Concrete Materials and Construction. Sustainable Concrete Construction. Proceedings of the International Conference held at the University of Dundee, Scotland, UK, September 9-11, 2002. pp. 805–818.

Wang, K., Zhi, G., Grove, J., Ruiz, J. M., and Rasmussen, R. 2006. *Developing a Simple and Rapid Test for Monitoring the Heat Evolution of Concrete Mixtures for Both Laboratory and Field Applications*. Phase I Report. National Concrete Pavement Technology Center, Iowa State University, Ames, IA.

Wang, K., Zhi, G., Grove, J., Ruiz, J. M., Rasmussen, R., and Ferragut, T. 2007. *Developing a Simple and Rapid Test for Monitoring the Heat Evolution of Concrete Mixtures for Both Laboratory and Field Applications*. Phase II Report. National Concrete Pavement Technology Center, Iowa State University, Ames, IA.